




Laser-based inertial fusion energy system enabled by optical enhancement cavities and a direct-drive configuration reactor

ATSUSHI SUNAHARA,*  GAURAV RAJ, TREVOR COHEN, P. MORGAN PATTISON, PAUL RUDY, YUYA OHARA, SEITA IIZUKA, HIROAKI OHTA, AND SHUJI NAKAMURA

Blue Laser Fusion, Inc., 6950 Hollister Ave. Goleta, CA 93117, USA

*asunahara@bluelaserfusion.com

Abstract: We propose a novel and highly efficient laser inertial fusion energy reactor concept based on the shock ignition scheme, in which laser-plasma instabilities are mitigated through 500-beam, multicolor, slowly rotating polarization laser beam irradiation. The system employs coherent beam-combined fiber lasers injected into high-finesse optical enhancement cavities, which have already demonstrated energy enhancement factors approaching 60,000 and are expected to surpass 100,000. The 1.06 μm laser output is frequency-tripled to 0.35 μm ultraviolet light, resulting in an overall wall-plug-to-ultraviolet-light efficiency of approximately 10%. The reactor integrates a helium-gas-cooled lead-lithium blanket and a direct energy conversion for high-efficiency operation. It is designed for cryogenic deuterium-tritium targets in a direct drive scheme at 1–10 Hz, repetition rate, providing net electric output at 0.1–2.8 GW. This approach offers a compact, scalable, and credible pathway toward practical commercial laser fusion energy.

Published by Optica Publishing Group under the terms of the [Creative Commons Attribution 4.0 License](https://creativecommons.org/licenses/by/4.0/). Further distribution of this work must maintain attribution to the author(s) and the published article's title, journal citation, and DOI.

1. Introduction

Blue Laser Fusion Inc. (BLF) was cofounded in California, USA, in 2022 by Prof. Shuji Nakamura, recipient of the 2014 Nobel Prize in Physics [1], shortly before the historic demonstration of net energy gain in laser inertial confinement fusion (ICF) at the National Ignition Facility (NIF) at Lawrence Livermore National Laboratory (LLNL) [2–5]. His invention of highly efficient blue LED [6] revolutionized global lighting by dramatically improving energy efficiency, which, in turn, reduced carbon emissions [7]. Building on this legacy, we are now working to address global energy and environmental challenges through the development of a laser fusion power reactor. Our core technology is based on Coherent Beam Combining (CBC) [8] in combination with Optical Enhancement Cavity (OEC) [9], which together will enable highly efficient and cost-effective megajoule-class pulsed laser systems operating at repetition rates up to 10 Hz by coherently injecting pulse trains from fiber lasers into the OEC.

The principles of the OEC have already been demonstrated in continuous-wave (CW) systems such as the Laser Interferometer Gravitational Wave Observatory (LIGO) [10,11] and other applications [12–17]. We are developing the OEC laser system to generate high-intensity, nanosecond-duration pulses for laser fusion applications and have already achieved significant power enhancement within the cavity [18]. We plan to scale up the CBC-OEC laser system to achieve a power enhancement factor of 100,000, enabling pulses of approximately 10 kJ per OEC module. By combining 500 such modules, we aim to construct a scalable 5 MJ-class laser system suitable for a practical fusion power reactor. This system will be used to irradiate cryogenic deuterium-tritium (DT) targets in a direct-drive ICF scheme. Our goal is to establish the first full-scale CBC-OEC prototype by 2027 and to demonstrate a pilot fusion reactor in the 2030s.

A related concept, the "StarDriver" design proposed by Eimerl et al. [19], envisioned more than 10,000 beams of 100 J each, amplified by DPSSL-pumped glass modules and spectrally broadened to suppress Laser-plasma instabilities (LPIs) [20]. While this approach shares with our CBC+OEC system the use of broadband multi-beam drivers for LPI mitigation, it faced major challenges in both cost and implementation. The reliance on glass amplifiers made the system relatively less cost-effective, and the extreme port density imposed severe constraints on chamber engineering, including blanket layout and heat-transfer system design. Moreover, as noted by Eimerl et al., fiber laser technology was not yet mature in 2014, preventing its use in that concept. By contrast, our approach coherently combines mass-produced fiber lasers and stores the energy in high-finesse optical enhancement cavities to generate 10 kJ per beam with 500 beams. This substantially reduces the number of external beams, relaxes both control-system and chamber-integration constraints, and provides a more cost-effective driver architecture while retaining the bandwidth and flexibility needed for advanced LPI suppression.

The main challenge in laser inertial fusion energy (IFE) [21] is to realize a plasma core with high density, high areal density, and high temperature, and to initiate thermonuclear burning, thereby efficiently achieving high fusion energy output. To achieve this, we adopt a slow implosion approach to mitigate the growth of hydrodynamic instabilities to attain a high areal density of the fuel, and then use the shock ignition scheme (SI) [22], which offers high gain. The fuel target is first slowly imploded using a relatively low intensity compression laser pulse to achieve high density and high areal density by keeping the inflight aspect ratio $R/\Delta R$ relatively small, thereby achieving high density and high areal density, where R and ΔR are the target radius and shell thickness, respectively. Subsequently, a high intensity ignition pulse is injected to launch a strong shock wave, generating high temperature and high density conditions by collision of shock waves near the center of the core, triggering thermonuclear burn [23]. Here, since the ignitor pulse has a significantly higher intensity than in conventional central ignition schemes, it is essential to suppress laser-plasma instabilities (LPIs), which can degrade the coupling of the laser energy [20].

Our BLF CBC-OEC laser system can generate pulses at high efficiency, 1–10 Hz repetition rate, and low cost with design flexibility to tune the pulse duration, pulse shape, effective spectral width, polarization state, and beam delivery configuration to the target. Using this flexibility, we aim to realize the LPI-mitigated SI for effectively achieving high-gain fusion energy output. The 500 beam CBC-OEC laser system provides significantly more uniform target illumination than conventional direct-drive laser fusion systems [24]. By superimposing beams with slightly shifted central wavelengths, the system achieves multicolor, effective broadband illumination, which helps mitigate LPIs. Additionally, by overlapping circularly polarized beams with different central wavelengths, a polarization state that rotates slowly over time, known as slowly rotating polarization (SRP) [25], is generated. This dynamic polarization modulation disrupts the spatial and temporal coherence required for LPI growth. Combined, these features provide robust suppression of LPIs, ensuring symmetric target compression and robust shock ignition. Furthermore, zooming is achieved by setting the compression pulse and ignition pulse at different focal points, allowing more laser energy to be coupled into the plasma.

By combining these innovative CBC-OEC laser techniques and irradiation configurations with shock ignition-based laser fusion, our approach aims to achieve a target gain exceeding 100, which is sufficient for practical laser fusion power generation. This enables the delivery of sub-GW to GW-class electric output through 5-MJ laser pulses at a repetition rate of 1–10 Hz. To support this performance, the reactor incorporates a magnetized dry wall chamber [26], which allows efficient and sustained repetition of the entire fusion cycle over extended operational periods, including injection of cryogenic DT targets, fusion burn, plasma exhaust handling, energy extraction, and tritium breeding.

This paper is structured as follows. Section 1 introduces the general concept; Section 2 describes the laser system; Section 3 discusses LPI-mitigated shock ignition; Section 4 presents the conceptual reactor design; and Section 5 provides a conclusion.

2. Laser system

Key requirements for commercialization include ultraviolet (UV) wavelength, pulse shaping control, spatial beam profile homogeneity, and broad bandwidth [27]. In addition, low production and maintenance costs, high reliability, MJ-class laser energy on the target, and a 1-10 Hz repetition rate are essential [21]. To meet these demanding requirements, we are developing a novel laser system architecture in which fiber-laser outputs are first coherently combined (CBC) [8] and then injected into an OEC [9].

Traditional solid-state amplifying technologies utilize large doped gain glass and either flash lamp or diode laser pump lasers to excite the amplifying medium. This approach is limited in repetition rate, requires large volumes of specialty gain glass panels, requires novel thermal management to avoid saturation, and requires extensive pump sources to achieve very high peak pulse power levels at very low repetition rates due to the required long cooling time [28].

In contrast, our CBC-OEC laser operates on a fundamentally different principle and represents a breakthrough in laser technology, capable of generating high-power laser pulses with high efficiency, low cost, and high repetition rates, as required for laser fusion. The core part of this laser system is a passive optical resonator that stores energy by coherently accumulating a train of externally injected laser pulses. This approach enables a compact system to deliver high power and high repetition rate without relying on a conventional gain medium. In this section, we describe the configuration of the CBC-OEC system, its operating principles, energy enhancement scaling, and the current status and roadmap for our laser development.

2.1. CBC-OEC configuration

Figure 1 shows the basic structure of the CBC-OEC laser module. This system coherently combines the laser output from many high-repetition-rate fiber lasers and injects a phase-coherent train of laser pulses into a Fabry–Pérot resonator formed by two highly reflective mirrors. The injected pulses constructively interfere through multiple reflections between the mirrors, resulting in efficient optical pulse stacking and energy buildup in the cavity. Owing to the high gain and compact single-pass configuration of fiber lasers, they can be easily parallelized to generate pulse trains with energy levels required for laser fusion implosions. Fiber amplifiers have superior cost scaling relative to gain glass media. Moreover, they allow for the precise temporal pulse shaping suitable for fusion applications.

Table 1 summarizes the characteristics of the laser output produced by the CBC-OEC module. As a laser source for IFE, the fiber lasers generate pulses at a wavelength λ of 1060 nm, with $\Delta\lambda$ of ± 10 nm and pulse duration of 0.1–10 ns, and inject them into the OEC. The OEC provides polarization flexibility, allowing selection between linear and circular polarization. Inside the cavity, the injected pulse train is coherently stacked to reach the desired high intensity. The resulting output, which exhibits an effective spectral bandwidth of 30 GHz, is extracted and subsequently wavelength-converted via second-harmonic generation (SHG) and third-harmonic generation (THG) to 0.53 μm and 0.35 μm , respectively. These UV pulses are then used for fusion target irradiation at repetition rates of 1–10 Hz.

2.2. Scaling of OEC

Efficient light storage in the OEC requires that the frequency components of the injected laser pulses match the resonant modes of the cavity. The round trip time T_R of the cavity is determined by its length L and the speed of light c , and is given by: $T_R = 2L/c$. This round trip time sets the injection repetition frequency: $f_{\text{rep}} = 1/T_R$. For example, a cavity length of 1.5 meters

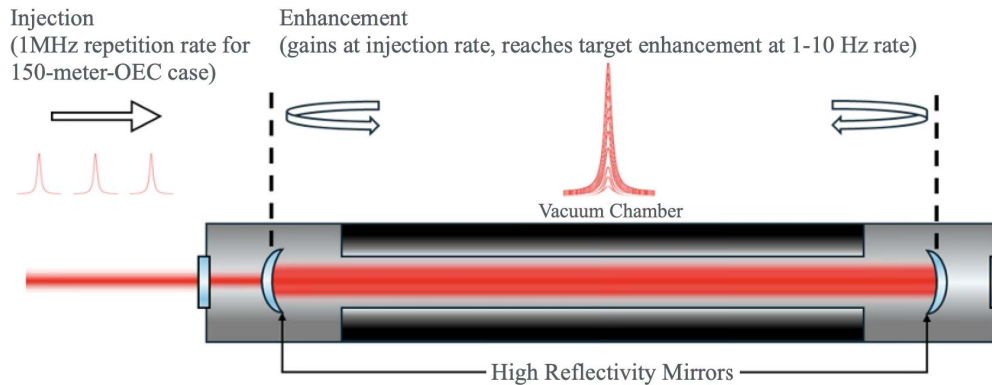


Fig. 1. Pulses stack internally to yield a single enhanced pulse. Schematic of the CBC-OEC laser module. A phase-coherent pulse train is injected into an optical enhancement cavity formed by highly reflective mirrors, where the pulses constructively interfere and accumulate, enabling high-intensity output for laser fusion applications.

Table 1. CBC-OEC Laser Pulse Conditions

Wavelength	λ	1060 nm
Changeable wavelength range	$\Delta\lambda$	± 10 nm
Pulse width	τ	0.1–10 ns
Polarization		Linear and circular
Effective bandwidth of the each OEC output	Δf	30 GHz
Wall-plug-to-light efficiency	η_w	0.16

corresponds to a repetition frequency f_{rep} of 100 MHz, whereas a 150-meter cavity corresponds to 1 MHz. When the repetition frequency of the injected pulse train matches f_{rep} , a coherent buildup of energy occurs inside the cavity. The free spectral range, defined as $\text{FSR} = 1/T_R = f_{\text{rep}}$, corresponds to the frequency spacing between adjacent longitudinal modes. When pulses are injected at intervals that match T_R , their temporal periodicity creates a frequency comb that overlaps with these cavity modes. An OEC can support a narrow but non-zero bandwidth of captive frequencies in the form of a frequency comb.

As L increases, the FSR decreases, allowing a larger number of modes to fit within the spectral bandwidth Δf of the pulse. Specifically, the number of resonant modes within the pulse bandwidth is approximately $\Delta f/\text{FSR}$. This improves spectral matching between the injected pulse train and the cavity resonances, enabling more efficient energy buildup. The enhancement factor, which is defined as the ratio of stored intra-cavity energy to injected energy, is governed by the finesse F , given by: $F = \pi/(T + A + S)$, where T , A , and S represent fractional losses per round trip due to mirror transmission, absorption, and scattering, respectively.

Minimizing these losses is essential to maximize finesse F and enhance cavity performance. Under ideal conditions with negligible internal losses, the finesse is primarily determined by the mirror reflectivity. With mirrors of reflectivity greater than or equal to 99.999% and an ultraclean vacuum environment, energy enhancement factors greater than 10^5 can be achieved at repetition rates of 1–10 Hz, as shown in Fig. 2.

While each mode of the frequency comb is as narrow as 1–5 Hz when the cavity finesse is high, the aggregate total of the modes sums up to a "bandwidth-in-parts" of $\Delta f = 30$ GHz. This bandwidth can be further enhanced if multiple OECs are used. Small tunable changes of the central wavelength, ranging from 1050–1070 nm wavelength to the spacing between the mirrors

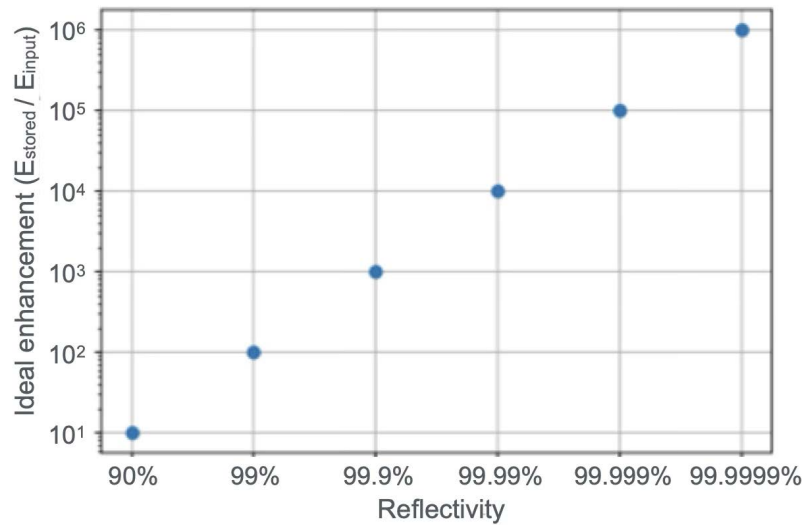


Fig. 2. Ideal enhancement in an OEC vs the mirrors' reflectivity

of each individual OEC, can result in a multitude of frequency combs, each spanning a slightly different range. These combs can then be combined by dumping the pulse out of the cavities which are directed to the overlapping irradiation on the fusion target as the multicolor, effective broadband light. Thus, the relative bandwidth $\Delta\omega/\omega_0 = |\Delta\lambda/\lambda|$ can be expanded to $\sim 1.9\%$ with multibeams, where $\omega_0 (= 2\pi c/\lambda)$ and $\Delta\omega$ are the angular frequency of the laser and its changeable range, respectively.

The ideal enhancement in an OEC builds up as a function of the number of incident pulses into the OEC. As the incident pulse, the pulse stacking begins gradually, grows exponentially, and eventually saturates. The ratio of power accumulated in the OEC to injected power reaches 75%. Consequently, the wall-plug-to-light efficiency of the CBC-OEC laser system η_w , defined as the ratio of electrical input to optical output at a wavelength of $1.06 \mu\text{m}$, is estimated to reach 16%.

We have assembled a meter-class, benchtop OEC to validate the concepts described above. Figures 3(a) and 3(b) show the high-quality beam profile and the vacuum chamber of the 1.5 m OEC in our US laser facility. High-finesse operation requires ultra-high reflectivity mirrors, minimized optical loss, and excellent thermal and mechanical stability. High-reflectivity mirrors with total optical losses below 10 ppm have already been experimentally demonstrated in the near- or mid-infrared spectral regions [29–33]. We have successfully constructed the high-finesse OEC prototype 1.5 m cavity using mirrors with more than 99.9995% reflectivity [18]. Under CW operation, this system achieved a finesse of 419,000 and an energy enhancement factor of 59,000. The design of the OEC is briefly described below. The benchtop OEC is a two-mirror, high-finesse, Fabry–Pérot cavity operated within a vacuum system. The vacuum system is comprised of two $0.3 \text{ m} \times 0.3 \text{ m} \times 0.3 \text{ m}$ aluminum cubes that house each of the cavity mirrors. The cubes are connected by a stainless-steel vacuum tube and pumped to a working pressure of approximately 1×10^{-5} torr by a turbomolecular pump from the center of the tube. The cavity mirrors are 2 inches in diameter with a measured transmission of $T = 3.4 \text{ ppm}$ by the coating vendors. These mirrors were mounted in stainless steel, vacuum-compatible mounts from Thorlabs.

A simplified diagram of the optical layout is shown in Fig. 4. The laser is injected into the OEC externally through one of the cavity mirrors that comprise the OEC. The output of a CW, 15 mW, wavelength tunable, 20 kHz bandwidth, vertically polarized, fiber laser is coupled to a

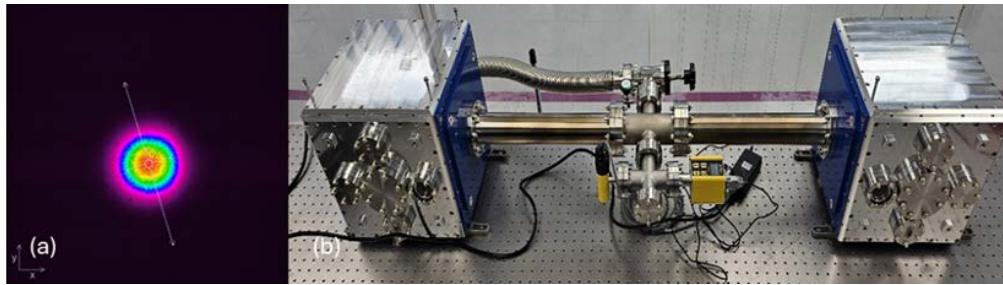


Fig. 3. (a) Beam profile of the transmission through the cavity when the laser is locked to the $TEM_{0,0}$ mode. The beam diameter is 3.2 mm (FWHM). (b) OEC vacuum chamber with 1.5 m cavity length [18].

30 GHz bandwidth, phase modulating fiber Electro-Optic Modulators (EOMs). This fiber EOM modulates the laser at approximately 20 MHz, generating two reference sidebands used for the PDH lock. The output of the two EOMs is directed into a fiber amplifier outputting a maximum of 1.2 W and collimated in free space.

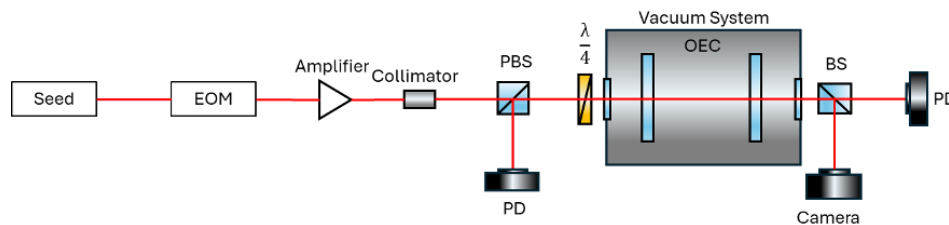


Fig. 4. A simplified optical layout of the 1.5 m OEC.

The laser is locked to the cavity using the Pound-Drever-Hall (PDH) method [34]. The cavity mirrors within the OEC are passively mounted without any feedback control. Feedback control is instead actuated on the laser, adjusting the output wavelength of the oscillator to match the cavity free spectral range. Sensing for the feedback mechanism is accomplished by a photodiode detector positioned to receive light rejected by the injection-side cavity mirror. The finesse of the cavity was evaluated by measuring the storage lifetime of the cavity through a cavity ringdown experiment, as described by Isogai et al. [35]. The finesse of a 2-mirror Fabry-Pérot cavity, F , can be calculated by the following formula: $F = 2\pi \times FSR \times \tau$, where τ is the lifetime the laser remains within the cavity. The length of the cavity was measured by a ruler to be 1.25 m and the free spectral range of the cavity was estimated by the formula: $FSR = \frac{c}{2L}$ to be 120 MHz.

The storage lifetime of the OEC, which is the time it takes for the light to exit the cavity by $1/e$ of the locked intensity, was measured by means of a cavity ringdown experiment. To measure τ , a 1 GHz response photodiode detector was positioned at the transmission end of the OEC, intercepting any laser light that leaks through both high reflectivity mirrors.

After locking the cavity and reaching a resonant steady state, the source laser is turned off, unlocking the cavity and resulting in the slow leak out of light from the cavity through both cavity mirrors. This leakage is observed on the photodiode detector as an exponential decay, which was fitted and was found to have a half-life of $557.5 \mu\text{s}$ in Fig. 5. The resultant finesse of the cavity was determined to be 419,000.

The enhancement factor of the cavity is a measure of the ratio of the average power circulating within the cavity and the power injected into the cavity. The power incident to the cavity and the power transmitted through the cavity while locked were measured to be 1.2 W and 240 mW,

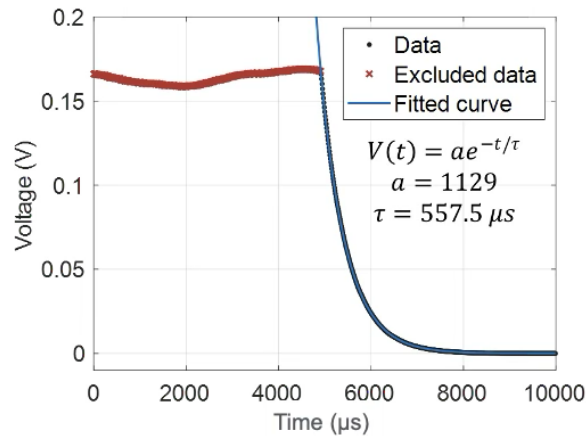


Fig. 5. The cavity ringdown of the OEC upon shutting off the injection laser entering the cavity.

respectively. The power circulating within the cavity while locked can be estimated as the power transmitted through the cavity divided by the transmission of the end cavity mirror. This was estimated to be 71 kW. While not all of the light is coupled to the cavity due to mode mismatch between the injection laser and the resonant $TEM_{0,0}$ mode of the cavity, we can conservatively estimate the enhancement factor of the cavity as 59,000 times.

The 15 meter long CBC-OEC systems are currently being constructed at both the Blue Laser Fusion Goleta site and Osaka University, as shown in Figs. 6(a)–6(c), targeting a pulse energy of 100 J and 10 kW injection laser.



Fig. 6. (a) the 15m OEC at the Goleta facility in the US, (b) an 8-channel CBC utilizing fiber rod amplifiers under construction, and (c) the 15 m OEC developed and built at the BLF Japan Osaka site.

2.3. Toward a reactor-scale laser

We plan to scale up the CBC-OEC system by increasing both the injection laser power and the optical storage capacity of the OEC, primarily through extending the cavity length. Figure 7 shows the output pulse energy as a function of the injection laser power for various cavity lengths. A 150-meter-scale cavity, capable of producing 10–16 kJ pulses 100 kW injection laser, is currently under design in collaboration with Caltech, Osaka University, and other partners. This configuration supports amplification factors up to 100,000, enabling the delivery of pulses at the reactor scale.

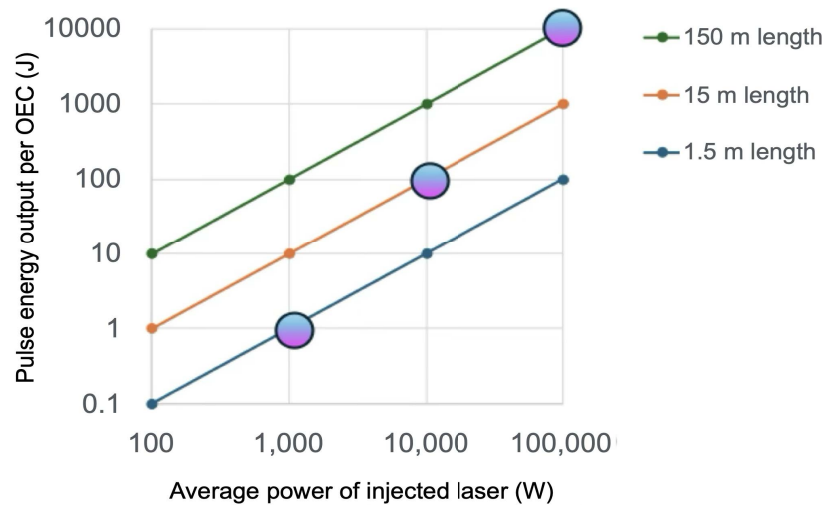


Fig. 7. BLF Laser-OEC power-energy-length stages. The pulse energy output per OEC as a function of the averaged power of the injected laser.

To meet these specifications, development efforts are focused on improving the vacuum system, high-reflectivity mirror alignment, thermal management, and active stabilization techniques. Enhanced optical coatings, precision mirror mounts, and real-time feedback control systems are being advanced to ensure stable and efficient operation under high thermal loads. In the 150-meter OEC configuration, each CBC-OEC laser module will coherently combine a 100 mJ, 1 MHz injection beam using mirrors with 99.9995% reflectivity. This architecture is being developed as a baseline laser driver for laser fusion reactors targeted for practical application in the early 2030s, with the first full-scale CBC-OEC prototype to be developed by 2027.

The purple markers in Fig. 7 indicate experimental milestones along the projected scaling trajectory. A gigawatt-scale laser IFE power plant can be realized by aggregating the outputs of 500 to 1,000 CBC-OEC modules, delivering 5 MJ of laser energy per shot at a repetition rate of 1–10 Hz to the fusion targets. The CBC-OEC platform offers a high degree of configurational flexibility, allowing precise control over polarization, phase, timing, pulse shaping, wavelength, and spectral bandwidth across all modules. This flexibility is critical for maximizing laser-plasma coupling efficiency and achieving the target gain necessary for practical, high-efficiency, gigawatt-class laser IFE power generation.

3. LPI-mitigation

In the SI, the initial target compression is driven by 5–10 ns laser pulses with moderate intensities ($I_{0c} \approx 5 \times 10^{14}$ W/cm²). In a later stage, the ignition shock is delivered by a much shorter pulse of duration $\tau_{0i} \approx 0.5$ –1 ns, but with significantly higher intensity ($I_{0i} \approx 10^{15}$ – 10^{16} W/cm²).

One of the main challenges in this scheme is the mitigation of LPIs [36,37], which arise from the interaction of laser beams with the dynamically evolving plasma corona surrounding the irradiated fuel target. Parametric LPIs such as stimulated Brillouin scattering (SBS), stimulated Raman scattering (SRS), two-plasmon decay (TPD), and cross-beam energy transfer (CBET) [20,38] can grow and saturate both linearly and nonlinearly, resonantly exciting secondary electromagnetic and electrostatic waves in the plasma corona with electron density n_e . As shown in Fig. 8, these LPIs occur in different density regions of the plasma corona and significantly modify the energy deposition and transport of the laser. Although such interactions often reduce

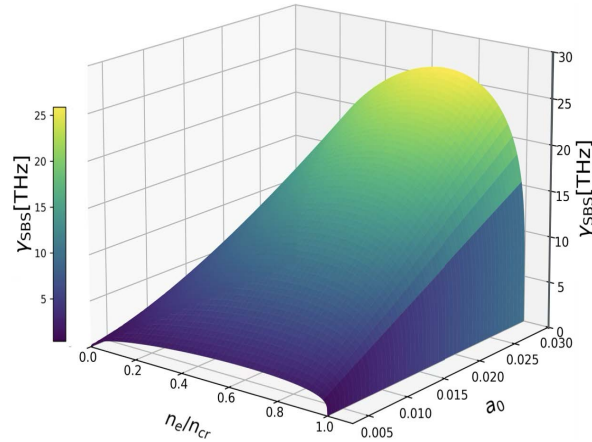


Fig. 9. Variation of the Back SBS instability growth rate γ_{SBS} with the laser strength parameter a_0 for $I_0 \approx 10^{14} - 10^{16} \text{ W/cm}^2$ and the plasma density n_e/n_{cr} .

compressed fuel and disrupt compression, whereas in SI, sub 100 keV electrons can be beneficial by enhancing the shock pressure during ignition [39,40], which is also confirmed experimentally [50].

Given the resonant nature of LPIs, any increase in the temporal incoherence, i.e. bandwidth, of the laser driver will disrupt the seeding and growth of the LPIs. Previous investigations have predicted that a large bandwidth can be effective in suppressing LPIs [51–54]. Recent numerical studies [55,56] show strong suppression of LPIs such as CBET, by using the frequency-tripled Nd:glass broadband laser with a bandwidth of ≈ 8 THz, ($\Delta\omega/\omega_0 \approx 1.0\%$ where $\Delta\omega = 2\pi\Delta f$). Another recent study shows that laser bandwidth can be used to increase threshold intensities for LPIs by minimizing the coherence time of broadband laser pulses with random spectral phases [56]. The 500 beam CBC-OEC laser system, to be constructed at the BLF site, can effectively deliver the relative bandwidth of $\Delta\omega/\omega_0 \sim 1.9\%$ (16 THz), which covers most of γ_{SBS} up to $a_0 = 0.025$ in Fig. 9, with multicolor illumination to the target, providing a unique framework for LPI suppression. The solid-state ultraviolet Fourth-generation Laser for Ultrabroadband eXperiments (FLUX) [57,58], recently built as a part of the OMEGA laser facility, is a high-bandwidth (15 THz) system which will be used to quantitatively test the effects of bandwidth on the LPIs. The FLUX can provide quantitative data for LPI suppression thresholds as a function of bandwidth, helping to validate the CBC-OEC strategy proposed here to realize LPI-mitigated SI.

Another important strategy for reducing the coherence between the laser beam and the plasma, thus suppressing the LPIs is to use Polarization Smoothing (PS) [59–63]. Recent experiments have shown that a simple polarization state (linear or circular) has no effect on reflection and transmission due to LPIs such as Back SBS [64]. However, for the case of laser beams with SRP, the overall reflectivity due to LPIs can be significantly reduced due to a reduction in the total interaction length [25]. In such a case of SBS the growth rate is given by $\gamma_{SBS} = a_0 c k_p \omega_{pi} / 4 [\omega_s \omega_0]^{-1/2} |\cos \Theta|$, where ω_s and ω_{pi} are the angular frequency of the scattered light and the ion plasma frequency, respectively, and $\Theta = \Theta(t, x)$ is the rotation angle of the polarization as a function of time and the 1D longitudinal spatial coordinate x . Particle-in-cell (PIC) simulations show that, for parameters similar to those of an ICF plasma, polarization rotation can reduce the SBS reflectivity by a factor of 5. To effectively reduce reflectivity, the rotation frequency of the polarization, $\Omega = |\omega_L - \omega_R|/2$ given by overlapping counter-rotating circularly polarized beams with angular frequencies of ω_L and ω_R [25], should match the dominant instability growth rate (e.g γ_{SBS}), corresponds to a rotation frequency in

the tens of THz range, but the reduction saturates for higher rotation frequencies ($\Omega \gg \gamma_{SBS}$). Since the future BLF, IFE reactor plans to use 500 OEC lasers, pairs of frequency-shifted, counter-rotating circularly polarized lasers can be used to generate SRP lasers, thus offering a novel approach to modulating laser pulses for suppressing LPI reflectivity, in ICF plasmas.

Furthermore, currently all high-power laser-based ICF experiments rely on "smoothed" laser beams, which use smoothing techniques such as random phase plates (RPP) [43,44,65,66] to introduce spatial incoherence into the beams. Such beams, on a coarse scale, show a smooth average intensity profile in their cross section, while on a fine laser wavelength scale they have a speckle structure statistical distribution of the speckle peak intensity [43,44,67]. RPP produces speckled laser beams with well-controlled and reproducible focal spot profiles with speckles fixed in space and modulated in time by the varying amplitude of the laser intensity, thus reducing any phase-front aberrations originating at the lens. From a time-domain viewpoint, the speckle pattern in the focal plane changes at a rate determined by the total bandwidth of the modulation, and thus, the time-integrated intensity seen by the plasma is smoothed. If this rate is faster than the plasma response time, it significantly suppresses the LPIs. Thus, the BLF OEC laser system offers a practical and scalable solution for mitigating LPIs in future laser IFE systems. These LPI mitigation strategies are essential to enable robust and efficient operation of the laser-plasma coupling in our reactor-scale architecture, discussed in Section 4.

4. Reactor

4.1. System configuration

Figure 10 illustrates the conceptual system of the prototype laser-driven inertial fusion energy power plant. This design leverages the innovative direct-drive, LPI-mitigated SI uniquely enabled by the CBC-OEC laser system. Each subsystem in this reactor is engineered to optimize energy conversion, support high-repetition operation of 1–10 Hz, and ensure reactor longevity.

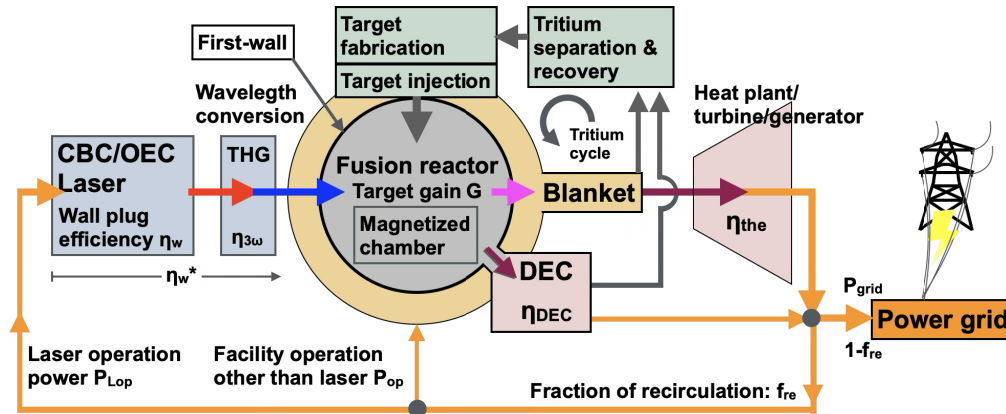


Fig. 10. Configuration of the laser IFE reactor

The wall-plug-to-light efficiency of the CBC-OEC laser at a wavelength of $1.06 \mu\text{m}$, denoted as η_w , is projected to be 0.16. Subsequently, these infrared pulses ($\lambda = 1.06 \mu\text{m}$) are frequency-tripled to UV light ($\lambda = 0.35 \mu\text{m}$) via THG in nonlinear optical crystals such as KDP/DKDP, with a typical conversion efficiency of $\eta_{3\omega} \approx 0.6$ [68]. The resulting overall wall-plug-to- $0.35 \mu\text{m}$ light efficiency is $\eta_w^* = \eta_w \times \eta_{3\omega} = 0.1$. The $0.35 \mu\text{m}$ UV light is used to irradiate cryogenic deuterium-tritium (DT) targets directly. The LPI-mitigated SI as described in the previous chapter employs 500-beam multicolor pulses, providing superior irradiation uniformity. Mostly, 360 beams are designated for compression and another 140 for ignition. SRP is generated by

overlapping counter-rotating circularly polarized beams with slightly different center wavelengths on the target. This temporal modulation of polarization interferes with the three-wave matching conditions required for LPI growth, thereby effectively suppressing SBS, SRS, and TPD, while irradiating the target uniformly. Additionally, the use of zooming and spatiotemporal pulse shaping further optimizes the laser-target energy coupling, contributing to higher implosion efficiency.

Approximately 70% of the fusion energy, carried by 14.1 MeV neutrons, is deposited in the blanket, which converts thermal energy to electricity via helium gas cooling and a conventional turbine generator. The blanket employs natural lithium (containing 7.5% ${}^6\text{Li}$ and 92.5% ${}^7\text{Li}$) as breeding material and a lead neutron multiplier (Pb). This configuration benefits from the volumetric flexibility of IFE systems compared to Tokamak magnetic fusion energy (MFE) reactors. The thermal-to-electric efficiency is assumed to be $\eta_{th} = 0.4$ with an additional 10% contribution from the exothermic ${}^6\text{Li}(n, \alpha)\text{T}$ reaction with tritium breeding, resulting in an effective $\eta_{th}^* = 0.44$. In the collaborative development of the blanket system with universities and national laboratories, we focus on a blanket using silicon-carbide (SiC)-based ceramics and cooling with helium gas, and we are investigating the possibility of integrating it with high temperature gas-cooled reactor (HTGR) technology [69,70], which has operating temperatures even higher than those envisioned for conventional nuclear fusion.

The remaining 30% of the fusion energy, associated alpha particles and plasma exhaust, are guided to direct electricity conversion (DEC) units [71–73] positioned along magnetic field lines. DEC systems utilize electrodes to extract electric power from ion kinetic energy. A conservative efficiency of $\eta_{DEC} = 0.44$ is assumed. Designs based on recent theoretical work [73] will be used to optimize ion collection geometries. DEC integration reduces the plant footprint and enhances overall system efficiency.

In addition, unlike Tokamak MFE reactors that store DT fuel in the reactor chamber, the amount of tritium in the IFE reactor chamber is limited to a few mg. Hence, the tritium cycle system dominates the tritium inventory of the entire reactor system for separating and recovering tritium from the blanket and plasma exhaust, and producing a new target and then injecting it into the reaction chamber at 1 to 10 Hz. Therefore, by designing the tritium cycle to increase the efficiency and speed of tritium processing, the tritium inventory of the system can be minimized. This approach reduces the risk of radioactive tritium leakage throughout the reactor system, supporting the realization of a safe fusion reactor.

The first wall should be designed to withstand impulsive loads from fusion-generated x-rays, alpha particles, and plasma debris. A layered structure is adopted, with tungsten (W) [74,75] as the facing material and reduced-activation ferritic-martensitic (RAFM) steel [76] as the structural support. Helium gas is used for active cooling. To mitigate the localized wall loading due to the deposition of charged particles, a chamber radius of 8–10 m is adopted, with embedded magnetic fields [75] to deflect alpha particles toward exhaust ports. Magnetic fields generated at each laser port provide magnetic fields within the dry-wall chamber. These magnetic fields serve to: (1) spread and decelerate ion trajectories, reducing thermal spot intensity and (2) redirect relatively low-energy plasma toward collection regions for DEC. Comprehensive magnetohydrodynamic (MHD) and particle-in-cell (PIC) simulations will be performed to optimize field geometry and wall survivability.

Reliable cryogenic DT target production at 1–10 Hz repetition rates is essential. Design specifications include: (1) Submicrometer surface roughness, (2) Uniform cryo-layering, (3) Positional accuracy, (4) Thermal shielding during flight. Although these are still major issues, development will continue with the aim of demonstrating power generation in early 2030. Component survivability under repetitive operation is a critical concern. Radiation-resistant optics, tungsten-based wall coatings, and modular component design are designed to be adopted. Remote handling and robotic inspection systems are incorporated for component replacement.

Survivability and radioactivation modeling of the first wall and chamber components will inform replacement intervals and long-term operational planning.

Unlike HiPER [77] and LIFE [78], which relied on DPSSL-driven glass amplifiers, our approach employs CBC of fiber lasers injected into OEC. This architecture is expected to substantially reduce the cost of the system and enable the straightforward implementation of broadband operation. In addition, in the LIFE design, the xenon-gas-protected dry-wall chamber wall was considered [79]. In contrast, the HiPER design adopted a vacuum dry-wall chamber, for which various plasma-facing materials (PFMs) were investigated [80]. Our reactor concept further advances these dry-wall approaches by applying an external magnetic field to mitigate the heat load on the first wall.

4.2. Power balance

The parameters related to the power flow in Fig. 10 are summarized in Table 2. The net fusion power output P_{fus} from laser irradiation of a target with laser energy E_L at a repetition rate f (Hz) and target gain G , is expressed as: $P_{fus} = E_L \times G \times f$. Of this total fusion energy, approximately 70% is carried by neutrons n [81] and captured in the blanket, where nuclear reactions with lead Pb as follows: $n + {}^{208}\text{Pb} \rightarrow {}^{207}\text{Pb} + 2n' - 7.4 \text{ MeV}$. Here, the number of neutrons is multiplied and the neutron emitted n' has a lower energy $\sim 1 \text{ MeV}$. This Pb has the reaction cross-section over 7 MeV of neutron energy. Also, 14.1 MeV neutrons can react with ${}^7\text{Li}$ over 2 MeV of neutron energy as follows [82]: ${}^7\text{Li} + n \rightarrow T + {}^4\text{He} + n'' - 2.8 \text{ MeV}$. Here, tritium T, alpha-particle ${}^4\text{He}$, and low-energy neutrons n'' are produced, respectively. Then, the relatively lower energy neutrons $< 2 \text{ MeV}$ can react with ${}^6\text{Li}$ to produce T and ${}^4\text{He}$ as follows: ${}^6\text{Li} + n \rightarrow T + {}^4\text{He} + 4.8 \text{ MeV}$.

Table 2. Key parameters for the power balance of the laser IFE reactor.

Variable	Symbol	Reactor value
Laser wavelength	λ_0	0.35 μm
Relative bandwidth with multicolor beam irradiation	$\Delta\omega/\omega_0$	1.9 %
Laser energy irradiating the target per shot	E_L	5 MJ
Laser operation frequency	f	1 to 10 Hz
CBC-OEC Laser wall-plug-to-light efficiency ($\lambda_L = 1 \mu\text{m}$)	η_w	0.16
Wavelength conversion efficiency, from 1 to 0.35 μm	$\eta_{3\omega}$	0.6
Overall wall-plug-to-0.35 μm light efficiency: $\eta_w^* = \eta_w \times \eta_{3\omega}$	η_w^*	0.1
Target gain = fusion energy output / laser energy input	G	160
Conversion efficiency to electricity via blanket	η_{the}	0.44
Direct Electricity Conversion efficiency	η_{DEC}	0.44
Total conversion efficiency from fusion to electricity: $\eta_e = 0.7\eta_{the} + 0.3\eta_{DEC}$	η_e	0.44
Facility operation power: (non-laser)	P_{op}	100 MW
Laser operation power $P_{Lop} = E_L \cdot f / \eta_w^*$	P_{Lop}	50 to 500 MW
Fraction of recirculation, [Eq. (1)]	f_{re}	0.426 to 0.170
Electricity power to grid, [Eq. (2)]	P_{grid}	102 to 2820 MW

These reactions release thermal energy, providing an additional 10% contribution of the thermal energy from the neutron-lithium reactions. The thermal energy is then used to drive a conventional turbine-generator system to produce electricity. Assuming a nominal thermal to electric conversion efficiency of $\eta_{th} = 0.4$, the effective conversion efficiency that includes the 10% thermal gain [27] becomes: $\eta_{th}^* = 1.1 \times \eta_{th} = 0.44$.

The remaining 30% of the fusion output, carried by alpha particles and other plasma exhaust [81], is guided to the lower exhaust ports of the chamber by the applied magnetic field. There, it is converted into electricity using a direct energy conversion (DEC) system that extracts electric power from the kinetic energy of particles. Since actual efficiency η_{DEC} depends heavily on the design, we conservatively assume: $\eta_{DEC} = \eta_{th}^* = 0.44$. Consequently, the total effective conversion efficiency from fusion to electricity, including both thermal and DEC channels, is given by: $\eta_{the}^* = 0.7 \times \eta_{th}^* + 0.3 \times \eta_{DEC} = 0.44$.

Also assuming a wall-plug-to-0.35 μm wavelength light efficiency of $\eta_w^* = 0.1$, the electrical power required to operate the laser is given by: $P_{Lop} = E_L \times f / \eta_w^*$. Furthermore, assuming the auxiliary facility operation power $P_{op} = 100$ MW, the fraction of the generated power consumed internally by the plant, the fraction of recirculating power f_{re} is calculated by:

$$f_{re} = \left[\frac{1}{\eta_w^*} + \frac{P_{op}}{E_L \cdot f} \right] \cdot \frac{1}{G \cdot \eta_e}. \quad (1)$$

Here, the first term in parentheses represents the laser operation, and the second term represents other plant systems. Assuming P_{op} is a constant independent of E_L or f , increasing the laser energy E_L and the repetition rate f decreases P_{op} 's relative contribution to the recirculation power. This indicates that, at higher laser throughput, the recirculating power is dominated by the laser system itself. For example, when $E_L = 5$ MJ and f is varied from 1 to 10 Hz, the recirculating power fraction, f_{re} , decreases from approximately 0.426 to 0.170. The net electric power delivered to the grid, P_{grid} , can be expressed as:

$$P_{grid} = (1 - f_{re}) \cdot E_L \cdot f \cdot G \cdot \eta_e - P_{op} \quad (2)$$

Thus, P_{grid} is strongly dependent on E_L , f , and G . According to the study by Froula et al. [56,83], the gain G as a function of the input laser energy E_L varies depending on the level of suppression of hydrodynamic instability and LPis, where three gain curves are reported: (i) baseline with instabilities, (ii) CBET-mitigated, and (iii) ideal 1D case with CBET-mitigated, respectively. As described in Section 3, our design employs 500 beams with relative bandwidth $\Delta\omega/\omega_0 \sim 1.9\%$, SRP light to achieve: (1) high uniform irradiation, (2) LPI mitigation strategies applicable to Direct Drive, and (3) independent focus (zooming) of compression and ignition pulses. Given this advanced configuration, we anticipate a higher target gain G beyond the CBET-mitigated curve of Froula (ii) and achieving a target gain of $G = 160$ at $E_L = 5$ MJ. Therefore, for a repetition rate of $f = 1-10$ Hz, the net deliverable electric power P_{grid} ranges from 102 MW to 2820 MW.

5. Conclusion

We have presented a new laser IFE reactor concept based on LPI-mitigated shock ignition enabled by the CBC-OEC. The CBC-OEC with >99.9995% reflectivity mirrors enables energy enhancement factors exceeding 59,000 and are projected to surpass 100,000 in scaled systems. This configuration achieves an overall wall-plug-to-UV light (0.35 μm) efficiency of 10%. To suppress LPis, which have been a long-standing barrier to direct-drive laser fusion, potentially in the SI, we employ an integrated strategy of 500-beam, multicolor, relative bandwidth $\Delta\omega/\omega_0 \sim 1.9\%$, SRP light irradiation with RPP and zooming. Together, these features enable exceptional irradiation uniformity and LPI mitigation, achieving target gains exceeding 160 at 5 MJ input. The reactor design incorporates a lithium-lead blanket cooled by helium gas and a direct energy conversion system for ion energy recovery. These combined systems yield a net thermal plus direct energy conversion efficiency exceeding 44%, enabling 0.1–2.8 GW_e net output at 1–10 Hz operation. The compact architecture, modularity, and limited tritium inventory support scalability, maintainability, and operational safety. This approach offers a realistic and scalable

path toward commercial laser fusion power. The continued advancement of high-repetition OEC platforms, integrated LPI suppression, and reactor subsystems is expected to enable net energy gain and gigawatt-class electricity generation within the next decade. Compared to conventional direct-drive or indirect-drive schemes, this approach leverages OEC-enabled optical architectures to reduce system size and improve energy coupling, offering a transformative and scalable path toward high-gain, high-repetition-rate laser fusion power plants.

Funding. This work was self funded by Blue Laser Fusion.

Acknowledgment. Preliminary OEC development support was provided by Professor Rana Adhikari of the California Institute of Technology under a 2024 DOE INFUSE grant.

Disclosures. The authors declare no conflict of interest.

Data availability. Data underlying the results presented in this paper are not publicly available at this time but may be obtained from the authors upon reasonable request.

References

1. J. Heber, "Nobel prize 2014: Akasaki, Amano & Nakamura," *Nat. Phys.* **10**(11), 791 (2014).
2. H. Abu-Shawareb, R. Acree, P. Adams, *et al.*, "Achievement of Target Gain Larger than Unity in an Inertial Fusion Experiment," *Phys. Rev. Lett.* **132**(6), 065102 (2024).
3. O. A. Hurricane, D. A. Callahan, D. T. Casey, *et al.*, "Energy Principles of Scientific Breakeven in an Inertial Fusion Experiment," *Phys. Rev. Lett.* **132**(6), 065103 (2024).
4. M. Rubery, M. Rosen, N. Aybar, *et al.*, "Hohlraum Reheating from Burning NIF Implosions," *Phys. Rev. Lett.* **132**(6), 065104 (2024).
5. A. Pak, A. Zylstra, K. Baker, *et al.*, "Observations and properties of the first laboratory fusion experiment to exceed a target gain of unity," *Phys. Rev. E* **109**(2), 025203 (2024).
6. S. Nakamura, T. Mukai, and M. Senoh, "High-power Gan P-N Junction Blue-Light-Emitting Diodes," *Jpn. J. Appl. Phys.* **30**(12A), L1998–L2001 (1991).
7. U.S. Department of Energy, "Energy Savings Forecast of Solid-State Lighting in General Illumination Applications," Tech. rep., Office of Energy Efficiency and Renewable Energy (2014). By 2030, LED lighting is projected to reduce electricity use for lighting by nearly 40% and avoid 198 million metric tons of CO₂ emissions annually.
8. V. Kozlov, J. Hernandez-Cordero, and T. Morse, "All-fiber coherent beam combining of fiber lasers," *Opt. Lett.* **24**(24), 1814–1816 (1999).
9. H. Stark, M. Müller, M. Kienel, *et al.*, "Electro-optically controlled divided-pulse amplification," *Opt. Express* **25**(12), 13494–13503 (2017).
10. J. Aasi, B. Abbott, R. Abbott, *et al.*, "Advanced LIGO," *Classical Quantum Gravity* **32**(7), 074001 (2015).
11. D. Ganapathy, W. Jia, M. Nakano, *et al.*, "Broadband Quantum Enhancement of the LIGO Detectors with Frequency-Dependent Squeezing," *Phys. Rev. X* **13**(4), 041021 (2023).
12. I. Chaikovska, K. Cassou, R. Chiche, *et al.*, "High flux circularly polarized gamma beam factory: coupling a Fabry-Perot optical cavity with an electron storage ring," *Sci. Rep.* **6**(1), 36569 (2016).
13. Z. Li, X. Deng, Z. Pan, *et al.*, "Generalized longitudinal strong focusing in a steady-state microbunching storage ring," *Phys. Rev. Accel. Beams* **26**(11), 110701 (2023).
14. X. Deng, A. Chao, J. Feikes, *et al.*, "Experimental demonstration of the mechanism of steady-state microbunching," *Nature* **590**(7847), 576–579 (2021).
15. B. Günther, R. Gradl, C. Jud, *et al.*, "The versatile X-ray beamline of the Munich Compact Light Source: design, instrumentation and applications," *Synchrotron Radiation* **27**(5), 1395–1414 (2020).
16. X.-Y. Lu, R. Chiche, K. Dupraz, *et al.*, "Stable 500 kW average power of infrared light in a finesse 35000 enhancement cavity," *Appl. Phys. Lett.* **124**(25), 251105 (2024).
17. X.-Y. Lu, R. Chiche, K. Dupraz, *et al.*, "710 kW stable average power in a 45,000 finesse two-mirror optical cavity," *Opt. Lett.* **49**(23), 6884–6887 (2024).
18. T. Cohen, J. Mance, S. Gandrothula, *et al.*, "Recent progress for commercializing IFE based on a novel high efficiency 10MJ laser and high-gain fuel target," *Optical Technologies for Inertial Fusion Energy* **13358**, 14–19 (2025).
19. D. Eimerl, E. M. Campbell, W. F. Krupke, *et al.*, "StarDriver: A Flexible Laser Driver for Inertial Confinement Fusion and High Energy Density Physics," *Journal of Fusion Energy* **33**(5), 476–488 (2014).
20. E. Campbell, V. Goncharov, T. Sangster, *et al.*, "Laser-direct-drive program: Promise, challenge, and path forward," *Matter Radiat. Extremes* **2**(2), 37–54 (2017).
21. National Research Council, Division on Engineering and Physical Sciences, Board on Energy and Environmental Systems, Board on Physics and Astronomy, Committee on the Prospects for Inertial Confinement Fusion Energy Systems, *An Assessment of the Prospects for Inertial Fusion Energy* (National Academies Press, 2013).
22. R. Betti, C. Zhou, K. Anderson, *et al.*, "Shock Ignition of Thermonuclear Fuel with High Areal Density," *Phys. Rev. Lett.* **98**(15), 155001 (2007).
23. S. Atzeni, X. Ribeyre, G. Schurtz, *et al.*, "Shock ignition of thermonuclear fuel: principles and modelling," *Nucl. Fusion* **54**(5), 054008 (2014).

24. T. Boehly, R. McCrory, C. Verdon, *et al.*, “Inertial confinement fusion experiments with OMEGA-A 30-kJ, 60-beam UV laser,” *Fusion Eng. Des.* **44**(1-4), 35–42 (1999).
25. I. Barth and N. J. Fisch, “Reducing parametric backscattering by polarization rotation,” *Phys. Plasmas* **23**(10), 102106 (2016).
26. L. A. Booth, D. A. Freiwald, T. G. Frank, *et al.*, “Prospects of Generating Power with Laser-Driven Fusion,” *Proc. IEEE* **64**(10), 1460–1482 (1976).
27. S. E. Bodner, “Comparison of an Argon-Fluoride Gas Laser with a Solid-State Laser for Application to Laser Fusion Energy,” *Journal of Fusion Energy* **42**(2), 33 (2023).
28. S. B. Sutton, A. Erlandson, R. A. London, *et al.*, “Thermal recovery of the NIF amplifiers,” in *Third International Conference on Solid State Lasers for Application to Inertial Confinement Fusion*, vol. 3492 (SPIE, 1999), pp. 665–675.
29. G. D. Cole, W. Zhang, B. J. Bjork, *et al.*, “High-performance near-and mid-infrared crystalline coatings,” *Optica* **3**(6), 647–656 (2016).
30. I. Ito, A. Silva, T. Nakamura, *et al.*, “Stable CW laser based on low thermal expansion ceramic cavity with 4.9 mHz/s frequency drift,” *Opt. Express* **25**(21), 26020–26028 (2017).
31. G. Wachter, S. Kuhn, S. Minniberger, *et al.*, “Silicon microcavity arrays with open access and a finesse of half a million,” *Light: Science Applications* **8**(1), 37 (2019).
32. G.-W. Truong, L. W. Perner, D. M. Bailey, *et al.*, “Mid-infrared supermirrors with finesse exceeding 400 000,” *Nat. Commun.* **14**(1), 7846 (2023).
33. J. Agil, B. Letourneur, S. George, *et al.*, “Characterisation of the waveplate associated to layers in interferential mirrors,” *The European Physical Journal Applied Physics* **98**, 61 (2023).
34. R. W. Drever, J. L. Hall, F. V. Kowalski, *et al.*, “Laser phase and frequency stabilization using an optical resonator,” *Appl. Phys. B* **31**(2), 97–105 (1983).
35. T. Isogai, J. Miller, P. Kwee, *et al.*, “Loss in long-storage-time optical cavities,” *Opt. Express* **21**(24), 30114–30125 (2013).
36. A. J. Schmitt and S. P. Obenschain, “The importance of laser wavelength for driving inertial confinement fusion targets. I. Basic physics,” *Phys. Plasmas* **30**(1), 012701 (2023).
37. A. J. Schmitt and S. P. Obenschain, “The importance of laser wavelength for driving inertial confinement fusion targets. II. Target design,” *Phys. Plasmas* **30**(1), 012702 (2023).
38. W. L. Kruer, *The Physics of Laser Plasma Interactions* (CRC Press, 2019).
39. W. Shang, R. Betti, S. Hu, *et al.*, “Electron Shock Ignition of Inertial Fusion Targets,” *Phys. Rev. Lett.* **119**(19), 195001 (2017).
40. W. Yuan, Z. Zhao, S. Zhu, *et al.*, “Nonlocal effects on the shock-augmented ignition scheme of laser inertial fusion,” *Phys. Rev. Res.* **6**(1), 013332 (2024).
41. I. V. Igumenshchev, W. Seka, D. H. Edgell, *et al.*, “Crossed-beam energy transfer in direct-drive implosions,” *Phys. Plasmas* **19**(5), 056314 (2012).
42. J. Moody, P. Michel, L. Divol, *et al.*, “Multistep redirection by cross-beam power transfer of ultrahigh-power lasers in a plasma,” *Nat. Phys.* **8**(4), 344–349 (2012).
43. G. Raj and S. Hüller, “Impact of Laser Beam Speckle Structure on Crossed Beam Energy Transfer via Beam Deflections and Ponderomotive Self-Focusing,” *Phys. Rev. Lett.* **118**(5), 055002 (2017).
44. S. Hüller, G. Raj, W. Rozmus, *et al.*, “Crossed beam energy transfer in the presence of laser speckle ponderomotive self-focusing and nonlinear sound waves,” *Phys. Plasmas* **27**(2), 022703 (2020).
45. L. Yin, K. L. Nguyen, B. J. Albright, *et al.*, “Effects of ion trapping and fluctuations of electron temperature and plasma flow on cross-beam energy transfer,” *Phys. Plasmas* **30**(10), 102703 (2023).
46. T. Boehly, D. Brown, R. Craxton, *et al.*, “Initial performance results of the OMEGA laser system,” *Opt. Commun.* **133**(1-6), 495–506 (1997).
47. V. N. Goncharov, T. Sangster, R. Betti, *et al.*, “Improving the hot-spot pressure and demonstrating ignition hydrodynamic equivalence in cryogenic deuterium–tritium implosions on OMEGA,” *Phys. Plasmas* **21**(5), 056315 (2014).
48. P. Michel, *Introduction to Laser-Plasma Interactions* (Springer Nature Switzerland AG, 2023).
49. M. N. Rosenbluth, “Parametric Instabilities in Inhomogeneous Media,” *Phys. Rev. Lett.* **29**(9), 565–567 (1972).
50. B. Yaakobi, A. A. Solodov, J. F. Myatt, *et al.*, “Measurements of the divergence of fast electrons in laser-irradiated spherical targets,” *Phys. Plasmas* **20**(9), 092706 (2013).
51. H. Baldis, E. Campbell, W. Kruer, *et al.*, “Handbook of Plasma Physics,” Elsevier Science, New York **1991**, 361–434 (1991).
52. W. L. Kruer, “Intense laser plasma interactions: From Janus to Nova,” *Phys. Fluids B* **3**(8), 2356–2366 (1991).
53. H. Yoneda, T. Miura, Y. Yokota, *et al.*, “Bandwidth effects on laser–plasma interaction with a 1/4- μm laser,” *Laser Part. Beams* **11**(1), 15–23 (1993).
54. A. Mostovych, S. Obenschain, J. Gardner, *et al.*, “Brillouin scattering measurements from plasmas irradiated with spatially and temporally incoherent laser light,” *Phys. Rev. Lett.* **59**(11), 1193–1196 (1987).
55. J. Bates, R. Follett, J. Shaw, *et al.*, “Suppressing cross-beam energy transfer with broadband lasers,” *High Energy Density Phys.* **36**, 100772 (2020).
56. D. H. Froula, C. Dorrer, A. Colaitis, *et al.*, “A future of inertial confinement fusion without laser-plasma instabilities,” *Phys. Plasmas* **32**(5), 052713 (2025).

57. C. Dorrer, E. M. Hill, and J. D. Zuegel, "High-energy parametric amplification of spectrally incoherent broadband pulses," *Opt. Express* **28**(1), 451–471 (2020).
58. C. Dorrer, M. Spilatro, S. Herman, *et al.*, "Broadband sum-frequency generation of spectrally incoherent pulses," *Opt. Express* **29**(11), 16135–16152 (2021).
59. E. M. Epperlein, "LLE Review Quarterly Report (October–December 1990), Volume 45," Tech. rep., Univ. of Rochester, NY (United States). Laboratory for Laser Energetics (1990).
60. E. Lefebvre, R. L. Berger, A. B. Langdon, *et al.*, "Reduction of laser self-focusing in plasma by polarization smoothing," *Phys. Plasmas* **5**(7), 2701–2705 (1998).
61. S. Skupsky and R. S. Craxton, "Irradiation uniformity for high-compression laser-fusion experiments," *Phys. Plasmas* **6**(5), 2157–2163 (1999).
62. T. R. Boehly, V. A. Smalyuk, D. D. Meyerhofer, *et al.*, "Reduction of laser imprinting using polarization smoothing on a solid-state fusion laser," *J. Appl. Phys.* **85**(7), 3444–3447 (1999).
63. K. Tsubakimoto, M. Nakatsuka, H. Nakano, *et al.*, "Suppression of interference speckles produced by a random phase plate, using a polarization control plate," *Opt. Commun.* **91**(1-2), 9–12 (1992).
64. J. G. Moreau, N. Blanchot, C. Rousseaux, *et al.*, "Stimulated Brillouin scattering dependence on polarization state, speckle shape, and polarization smoothing implementation," *Phys. Plasmas* **32**(3), 032102 (2025).
65. S. M. Hamadani, F. Soltanmoradi, M. H. Marvasti, *et al.*, "Laser plasmas," *Appl. Phys. B* **29**(3), 186–188 (1982).
66. H. A. Rose and D. F. DuBois, "Initial development of ponderomotive filaments in plasma from intense hot spots produced by a random phase plate," *Phys. Fluids B* **5**(9), 3337–3356 (1993).
67. H. A. Rose and D. F. DuBois, "Statistical properties of laser hot spots produced by a random phase plate," *Phys. Fluids B* **5**(2), 590–596 (1993).
68. P. J. Wegner, J. M. Auerbach, C. E. Barker, *et al.*, "Frequency converter development for the National Ignition Facility," in *Third International Conference on Solid State Lasers for Application to Inertial Confinement Fusion*, vol. 3492 (SPIE, 1999), pp. 392–405.
69. A. Koster, H. Matzner, and D. Nicholsi, "PBMR design for the future," *Nucl. Eng. Des.* **222**(2-3), 231–245 (2003).
70. K. Nagatsuka, H. Noguchi, S. Nagasumi, *et al.*, "Current status of high temperature gas-cooled reactor development in Japan," *Nucl. Eng. Des.* **425**, 113338 (2024).
71. A. Haught, "Magnetic Field Confinement of Laser Irradiated Solid Particle Plasmas," in *Laser Interaction and Related Plasma Phenomena: Volume 2 Proceedings of the Second Workshop, held at Rensselaer Polytechnic Institute, Hartford Graduate Center, Hartford, Connecticut, August 30–September 3, 1971*, (Springer, 1972), pp. 289–289.
72. Y. P. Zakharov, A. V. Melekhov, V. G. Posukh, *et al.*, "Direct Conversion of the Energy of Laser and Fusion Plasma Clouds to Electrical Energy During Expansion in a Magnetic Field," *Journal of Applied Mechanics and Technical Physics* **42**(2), 185–195 (2001).
73. J.-M. Rax, E. Kolmes, and N. Fisch, "Efficiency and Physical Limitations of Adiabatic Direct Energy Conversion in Axisymmetric Fields," *PRX Energy* **4**(1), 013007 (2025).
74. J. Sethian, A. Raffray, J. Latkowski, *et al.*, "Considerations for the chamber first wall material in a laser fusion power plant," *J. Nucl. Mater.* **347**(3), 161–177 (2005).
75. M. W. McGeoch and S. P. Obenschain, "Direct Drive Laser Fusion Facility and Pilot Plant," *Journal of Fusion Energy* **43**(2), 23 (2024).
76. S. M. G. De Vicente, N. A. Smith, L. El-Guebaly, *et al.*, "Overview on the management of radioactive waste from fusion facilities: ITER, demonstration machines and power plants," *Nucl. Fusion* **62**(8), 085001 (2022).
77. B. Le Garrec, M. Novaro, M. Tyldesley, *et al.*, "HiPER laser reference design," *Proc. SPIE* **8080**, 80801V-1–80801V-9 (2011).
78. M. Dunne, E. Moses, P. Amendt, *et al.*, "Timely delivery of laser inertial fusion energy (LIFE)," *Fusion Sci. Technol.* **60**(1), 19–27 (2011).
79. J. F. Latkowski, R. P. Abbott, S. Aceves, *et al.*, "Chamber design for the laser inertial fusion energy (LIFE) engine," *Fusion Sci. Technol.* **60**(1), 54–60 (2011).
80. R. Gonzalez-Arrabal, A. Rivera, and J. Perlado, "Limitations for tungsten as plasma facing material in the diverse scenarios of the European inertial confinement fusion facility HiPER: Current status and new approaches," *Matter Radiat. Extremes* **5**(5), 055201 (2020).
81. T. Johzaki, Y. Nakao, H. Nakashima, *et al.*, "Effects of neutron heating on ignition and energy gain of laser-imploded DT pellets," *Laser Part. Beams* **15**(2), 259–276 (1997).
82. H. M. Şahin, G. Tunç, A. Karakoç, *et al.*, "Neutronic study on the effect of first wall material thickness on tritium production and material damage in a fusion reactor," *Nucl. Sci. Tech.* **33**(4), 43 (2022).
83. R. Follett, A. Colaitis, I. Igumenshchev, *et al.*, "An experimentally informed design process for future inertial confinement fusion facilities," *Phys. Plasmas* **32**(4), 042705 (2025).